principal strain of an element was less than -10000 microstrain. Vertebral yield was defined as being when at least one element yielded, and vertebral fracture was defined as being when at least one element failed. The yield load, the fracture load, the sites where elements failed and the distribution of minimum principal strain were analyzed.

Quasi-static uniaxial compressive load testing

To verify the simulations, a quasi-static uniaxial compression test of each vertebra was conducted. Load, cross-head displacement, and principal strain at the vertebral surface were measured. To restrain the specimens for load testing, both upper and lower surfaces of the vertebrae were embedded in dental resin (Ostron; GC Dental Products Co., Aichi, Japan) so that the two surfaces were exactly parallel. Then the embedded specimens were placed on a mechanical testing machine (TENSILON UTM-2.5T; Orientec, Tokyo, Japan) and were compressed at a cross-head displacement rate of 0.5 mm per minute. A compression plate with a ball joint was used to apply a uniform load onto the upper surface of the specimen. The applied load was measured by a load cell (T-CLB-5-F-SR; T. S. Engineering, Kanagawa, Japan). The load and the cross-head displacement were recorded using MacLab/4 (AD Instruments, Castle Hill, NSW, Australia) at a sampling rate of 2 Hz. For 9 of the 12 vertebrae, one of the four rosette strain gauges (SKF-22358; Kyowa Electronic, Tokyo, Japan) was attached to each of anterior, left, right and posterior surfaces of the vertebra. The strain

readings were recorded at a sampling rate of 0.5 Hz and stored by a data logger (U-CAM-20PC-1; Kyowa Electronic); then, principal strain was calculated at each of the attachment sites. The measured yield load was defined as the load that reached the end of the plateau of the constant load increment rate, which corresponded with the end of the linear phase on the load displacement curve. The measured fracture load was defined as the ultimate load achieved (Fig. 2). To determine the actual fracture sites, antero-posterior and lateral soft X-ray pictures (Softex, Kanagawa, Japan) and micro-CT (MCT-CB100MF: Hitachi Medico Technology Corporation, Tokyo, Japan) images scanned with 70 kV, 100 μA, and a voxel size of 107 μm were obtained after the mechanical testing. The micro-CT images were processed and reconstructed to obtain the images at the mid-sagittal cross section and at the mid-frontal cross section. The sites and the types of experimental fractures were judged from the soft X-ray pictures and the reconstructed micro-CT images.

A 3D surface acquisition system using an image encoder (VOXELAN; Hamano Engineering, Kanagawa, Japan) was employed to identify the gauge attachment sites on the shell elements by matching the 3D surface image with the FE model. All three images, i.e., the 3D mesh model, the 2D digitized image, and the 3D surface image, were matched and the strain gauge attachment sites were then identified (Fig. 3). The minimum principal strain was calculated with an applied load of 1000 N, under which all specimens were in the elastic phase.

Pearson's correlation analysis was used to evaluate correlations between the predicted and the measured fracture loads, as well as between the predicted and the measured minimum principal strains.

Results

There was a significant linear correlation between the yield loads predicted by the FE analysis and those of the measured ($r = 0.949$, $p < 0.0001$) (Fig. 4). The correlation between the FE predicted fracture loads and the measured was even stronger ($r = 0.978$, $p < 0.0001$), and the slope of the regression line was 0.8807 (Fig. 5). There was also a significant linear correlation between the FE predicted minimum principal strain and the measured ($r = 0.838$, $p < 0.0001$) (Fig. 6).

There were two types of experimental fractures. Obvious fracture lines were recognized in six vertebrae. There were no obvious fracture lines in the other six, but they had apparent residual deformities after the mechanical testing. The anterior part of the vertebra was compressed in three out of the six. The other two sustained middle part compression and in one there was compression of the entire vertebra.

The experimental fracture line in the specimen was found to pass through a region of the failed elements on the simulation model (Fig. 7). In addition, the FE analysis of the minimum principal strain at the mid-sagittal section disclosed that the area with a large absolute value of

this predicted minimum principal strain agreed well with the experimental fracture site and that it visualized the fractured area.

In the specimens with anterior compression, marked radiolucency was recognized at the anterior part of the vertebra, where the trabecular pattern was observed to be very coarse (Fig. 8). The FE analysis showed that the failed elements appeared at the same anterior part as the area with coarse trabeculae. Likewise, the area with large absolute value of the minimum principal strain localized at the anterior part, which agreed with the area of the experimental compression fracture.

Discussion

The correlations between the measured values of fracture strength and the predicted values with the FE model were very good ($r = 0.978$) and better than the previous FE studies ($r = 0.89$-0.95). The characteristics of the FE model in this study were as follows: adoption of tetrahedron elements to precisely model surface curvatures of the entire vertebra, utilization of nonlinear analysis to match the elastoplasticity of the vertebra in compression, construction of cortical shells on the surface of the model, and adoption of Drucker-Prager equivalent stress instead of von-Mises stress as a criterion of an element yield. Which of these factors contributed most to the results was not determined in this study, because we did not separate these characteristics to analyze each factor's contribution. Clarification of this feature will be

one of our targets for the next study.

With tetrahedron elements, it was possible to create a more proximate, realistic and smooth surface contour than with hexahedral elements, which could possibly avoid any artificial stress raisers.

With the currently available CT resolution, strength of the cortical shell tended to be underestimated. In CT-based FE models, density of this shell has been underestimated because it is dependent on its Hounsfield unit value. It has been reported that in previous experiments thin cortical shell of the vertebrae contributed approximately 10% to the overall vertebral strength in healthy individuals and the contribution of the cortical shell was estimated to be significantly larger in osteoporotic individuals [2, 30]. Thus, the importance of the strength of the cortical shell should be taken into consideration in predicting the fracture load of osteoporotic individuals.

Overaker et al. set the thickness of the anterior cortex as 0.6 mm and that of the posterior as 0.4 mm; they set the cortical Young's modulus as 5, 6, 7 GPa. They concluded that Young's modulus of 7 GPa precisely correlated with the experimental result [29]. Liebschner et al. set the thickness as 0.35 mm and Young's modulus as 0.475 GPa. [15]. We constructed a cortical shell with a thickness of 0.4 mm and Young's modulus of 10 GPa. The cortical area with a thickness of more than 0.4 mm was modeled with both the shell and the tetrahedron element adjacent to the shell.

Young's modulus of human cortical bone has been reported to be 15 GPa [31], 19.9 GPa (dynamic) and 16.2 GPa (static) [32]. Young's modulus of human vertebra cancellous tissue was reported as 3.8-13.4 GPa [25-28] but few data of cortical shell have been available. Thus, it was necessary to set our own value. Young's modulus of the cortical shell obtained from the QCT data was 7 GPa. QCT underestimated the cortical shell density, so the actual density was estimated to be higher than that derived from QCT. Therefore, we set Young's modulus as 10 GPa, and then the values of the minimum principal strain were accurately predicted with a correlation coefficient of 0.838 and a slope of the regression line of 0.9288.

In previous studies, von Mises equivalent stress has been used as the criterion of yield [8, 10, 13]. For ductile materials such as metals, von Mises criterion would be effective, but for bones it seems more appropriate to use Drucker- Prager equivalent stress. The yield strain of human vertebral trabecular bone was reported -7000 to -10000 microstrain [17, 18]. Therefore, we adopted minimum strain of -10000 microstrain as a criterion for element collapse.

Some previous reports described the mechanical properties of human bone. We tested three theories: Carter and Hayes' property [33, 34], Keller's [35], and Keyak's [10]. With Carter and Hayes' property, the predicted fracture loads were about 60 % and using Keller's, the predicted fracture loads were about 120 % of those of the experiment. Accurate prediction could be made with Keyak's, although further investigations will be necessary to obtain the actual mechanical properties of human vertebra.

In this investigation, prediction of the ultimate load was more accurate than that of the yield load. One possibility was that determination of the experimental yield load was not appropriate. The ultimate load was clearly determined, but the yield load was objectively determined from load versus displacement curves by calculating the load increment rate (Fig.2).

There were two types of vertebral fracture: one showed fracture line and the other showed no fracture lines but had apparent residual deformities. Both fracture types could be predicted. Fracture location was most accurately predicted by the distribution of very low levels of the minimum principal strain. Therefore, we speculated that fracture was initiated at the sites of failed elements and propagated along with the area with very low minimum principal strain.

The prediction was made under a very simple loading condition with quasi-static uniaxial vertical loading. The condition was the simplest but it minimized experimental error which might have occurred to some degree with complicated loading conditions. Arbitrary load magnitude or direction can be set for the same simulation model. So it is possible to analyze strength or fracture site of vertebrae for loading conditions which actually cause fractures, although it would be very hard to create these fractures under an experimental condition. To predict in vivo behavior of spinal bones is another target for our next study.

To verify our model, we evaluated three factors; fracture strength, fracture site, and strain on the surface of the vertebrae. Prediction of only fracture strength would not be adequate to evaluate the accuracy of FE analysis. Predicted fracture sites should also be matched with those of the experiment, and the process by which deformation of the vertebrae proceeds should be simulated. To attain this, we used strain gauges to measure surface strain throughout the loading process. This has not been done in previous studies investigating the accuracy of a simulation model.

The limitation is the cortical shell was treated as a homogenous material because the pixel spacing with CT is too large to model the thin cortical shell. If a CT with improved resolution becomes available, it would make it possible to model the cortical shell with heterogeneous properties, thus enabling creation of a more realistic model.

There is another limitation. The posterior portion of the vertebra was excised in this study. A 3D surface acquisition system using an image encoder was employed to identify the gauge attachment sites on the shell elements. With the posterior portion of the vertebra such as lamina or spinous process, obtaining 3D surface image of the posterior part of the vertebral body should be interfered. It was one of the reasons why the posterior portion of the vertebra was excised. Clinically, most of the vertebral fractures occur at the vertebral body. However, the posterior portion of the vertebra might share some ratio of axial loading. Therefore, loading environment in in vivo situation may be different from that in this study. To predict in

vivo behavior of spinal bones, the posterior portion of the vertebra must be included.

The cadaveric specimens were all extracted from males, whose bone quality might be somewhat different from that of females. To utilize this model as a diagnostic tool for osteoporosis, it would have been better to use specimens from both males and females. Validation of accurate prediction by the FE model in an experiment using female cadaveric specimens will be another target of our future study. Furthermore, true efficacy of this method will be validated after a large-scale cohort study investigating the relationship between the predicted fracture loads in the study groups and the occurrence rates of actual fracture in the same groups. It is expected that this method will be valuable in estimating fracture risk of vertebrae in osteoporotic individuals.

References

1. Mosekilde L, Bentzen SM, Ortoft G, et al. The predictive value of quantitative computed tomography for vertebral body compressive strength and ash density. Bone 1989; 10: 465-70.

2. McBroom RJ, Hayes WC, Edwards WT, et al. Prediction of vertebral body compressive fracture using quantitative computed tomography. Journal of Bone and Joint Surgery 1985; 67-A: 1206-14.

3. Brinckmann P, Biggemann M, Hilweg D, et al. Prediction of the compressive strength of human lumbar vertebrae. Clinical Biomechanics 1989; 4: S1-27.

4. Edmondston SJ, Singer KP, Day RE, et al. In-vitro relationships between vertebral body density, size and compressive strength in the elderly thoracolumbar spine. Clinical Biomechanics 1994; 9: 180-6.

5. Cheng XG, Nicholson PH, Boonen S, et al. Prediction of vertebral strength in vitro by spinal bone densitometry and calcaneal ultrasound. Journal of Bone and Mineral Research 1997; 12: 721-8.

6. Myers BS, Arbogast KB, Lobaugh B, et al. Improved assessment of lumbar vertebral body strength using supine lateral dual-energy x-ray absorptiometry. Journal of Bone and Mineral Research 1994; 9: 687-93.

7. Bjarnason K, Hassager C, Svendsen OL, et al. Anteroposterior and lateral spinal DXA for the assessment of vertebral body strength: comparison with hip and forearm measurement. Osteoporosis International 1996; 6: 37-42.

8. Lotz JC, Cheal EJ, Hayes WC. Fracture prediction for the proximal femur using finite element models: Part I--Linear analysis. Journal of Biomechanical Engineering 1991; 113: 353-60.

9. Lotz JC, Cheal EJ, Hayes WC. Fracture prediction for the proximal femur using finite element models: Part II--Nonlinear analysis. Journal of Biomechanical Engineering 1991; 113: 361-5.

10. Keyak JH, Rossi SA, Jones KA, et al. Prediction of femoral fracture load using automated finite element modeling. Journal of Biomechanics 1998; 31: 125-33.

11. Keyak JH. Improved prediction of proximal femoral fracture load using nonlinear finite element models. Medical Engineering & Physics 2001; 23: 165-73.

12. Cody DD, Gross GJ, Hou FJ, et al. Femoral strength is better predicted by finite element models than QCT and DXA. Journal of Biomechanics 1999; 32: 1013-20.

13. Silva MJ, Keaveny TM, Hayes WC. Computed tomography-based finite element

analysis predicts failure loads and fracture patterns for vertebral sections. Journal of Orthopaedic Research 1998; 16: 300-8.

14. Martin H, Werner J, Andresen R, et al. Noninvasive assessment of stiffness and failure load of human vertebrae from CT-data. Biomedizinische Technik 1998; 43: 82-8.

15. Liebschner MA, Kopperdahl DL, Rosenberg WS, et al. Finite element modeling of the human thoracolumbar spine. Spine 2003; 28: 559-65.

16. Crawford RP, Cann CE, Keaveny TM. Finite element models predict in vitro vertebral body compressive strength better than quantitative computed tomography. Bone 2003; 33: 744-50.

17. Keaveny TM, Wachtel EF, Ford CM, et al. Differences between the tensile and compressive strengths of bovine tibial trabecular bone depend on modulus. Journal of Biomechanics 1994; 27: 1137-46.

18. Kopperdahl DL, Keaveny TM. Yield strain behavior of trabecular bone. Journal of Biomechanics 1998; 31: 601-8.

19. Morgan EF, Keaveny TM. Dependence of yield strain of human trabecular bone on anatomic site. Journal of Biomechanics 2001; 34: 569-77.

20. Silva MJ, Wang C, Keaveny TM, et al. Direct and computed tomography

thickness measurements of the human, lumbar vertebral shell and endplate. Bone 1994; 15: 409-14.

21. Vesterby A, Mosekilde L, Gundersen HJ, et al. Biologically meaningful determinants of the in vitro strength of lumbar vertebrae. Bone 1991; 12: 219-24.

22. Mosekilde L. Vertebral structure and strength in vivo and in vitro. Calcified Tissue International 1993; 53: S121-6.

23. Dougherty G, Newman D. Measurement of thickness and density of thin structures by computed tomography: a simulation study. Medical Physics 1999; 26: 1341-8.

24. Prevrhal S, Engelke K, Kalender WA. Accuracy limits for the determination of cortical width and density: the influence of object size and CT imaging parameters. Physics in Medicine and Biology 1999; 44: 751-64.

25. Jensen KS, Mosekilde L. A model of vertebral trabecular bone architecture and its mechanical properties. Bone 1990; 11: 417-423.

26. Rho JY, Tsui TY, Pharr GM. Elastic properties of human cortical and trabecular lamellar bone measured by nanoindentation. Biomaterials 1997; 18: 1325-1330.

27. Hou FJ, Lang SM, Hoshaw SJ, et al. Human vertebral body apparent and hard

tissue stiffness. Journal of Biomechanics 1998; 31: 1009-1015.

28. Ladd AJ, Kinney JH, Haupt DL, et al. Finite-element modeling of trabecular bone: comparison with mechanical testing and determination of tissue modulus. Journal of Orthopaedic Research 1998; 16: 622-628.

29. Overaker DW, Langrana NA, Cuitino AM. Finite element analysis of vertebral body mechanics with a nonlinear microstructural model for the trabecular core. Journal of Biomechanical Engineering 1999; 121: 542-50.

30. Faulkner KG, Cann CE, Hasegawa BH. Effect of bone distribution on vertebral strength: assessment with patient-specific nonlinear finite element analysis. Radiology 1991; 179: 669-74.

31. Choi K, Kuhn JL, Ciarelli MJ, et al. The elastic moduli of human subchondral, trabecular, and cortical bone tissue and the size-dependency of cortical bone modulus. Journal of Biomechanics 1990; 23: 1103-13.

32. Katsamanis F, Raftopoulos DD. Determination of mechanical properties of human femoral cortical bone by the Hopkinson bar stress technique. Journal of Biomechanics 1990; 23: 1173-84.

33. Carter DR, Hayes WC. Bone compressive strength: the influence of density and strain rate. Science 1976; 194: 1174-6.

34. Carter DR, Hayes WC. The compressive behavior of bone as a two-phase porous structure. Journal of Bone and Joint Surgery 1977; 59-A: 954-62.

35. Keller TS. Predicting the compressive mechanical behavior of bone. Journal of Biomechanics 1994; 27: 1159-68.

Fig. 1

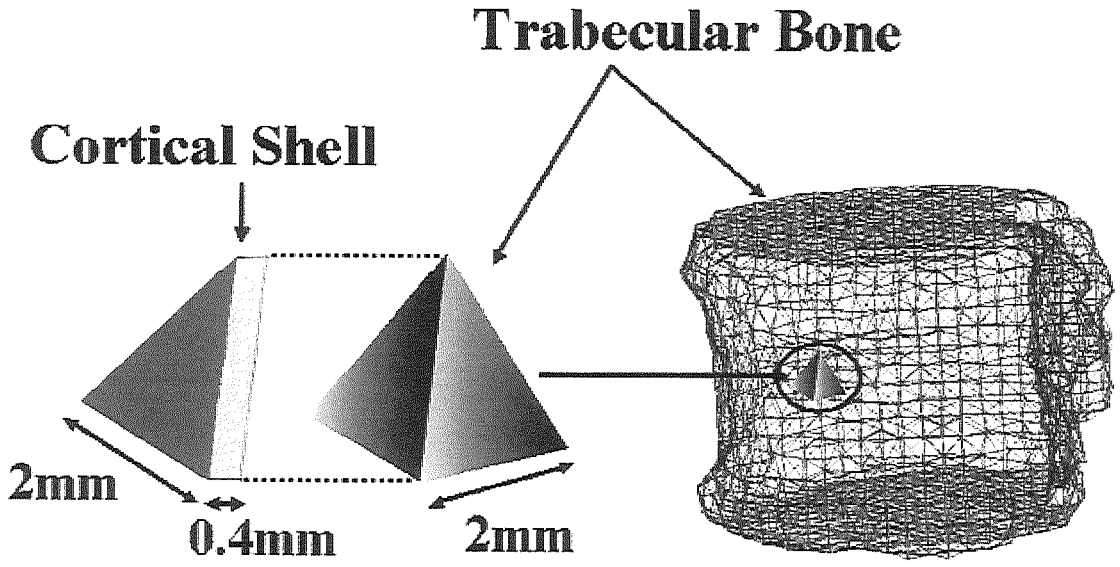

Fig. 2

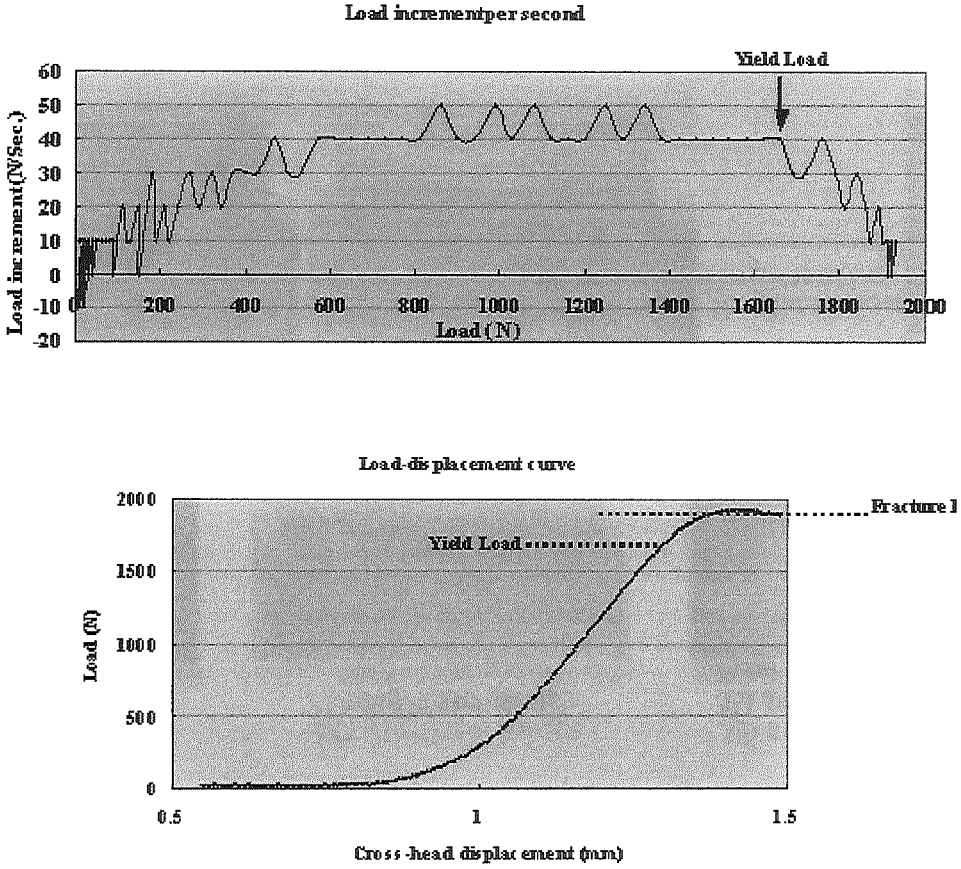
Load increment per second
Yield Load
Load increment(N/Sec.)
60
50
40
30
20
10
0
-10
-20
0
200
400
600
800
1000
1200
1400
1600
1800
2000
Load (N)
Load-displacement curve
Fracture l
Yield Load
Load (N)
2000
1500
1000
500
0
0.5
1
1.5
Cross-head displacement (mm)

Fig. 3

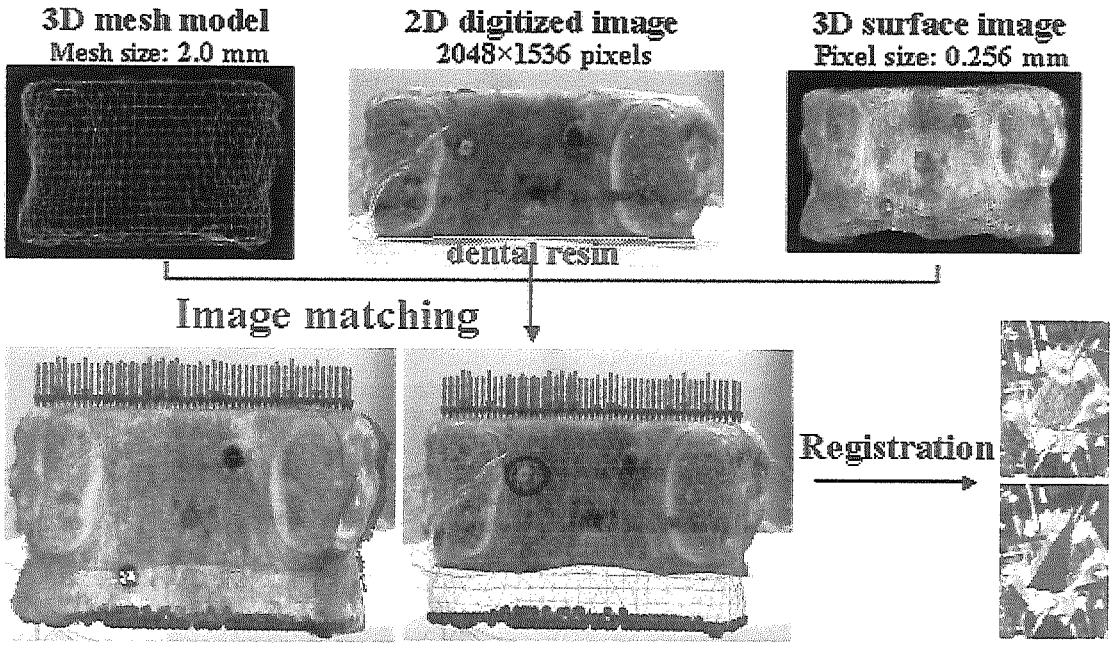
3D mesh model
Mesh size: 2.0 mm
2D digitized image
2048×1536 pixels
3D surface image
Pixel size: 0.256 mm
dental resin
Image matching
Registration

Fig. 4

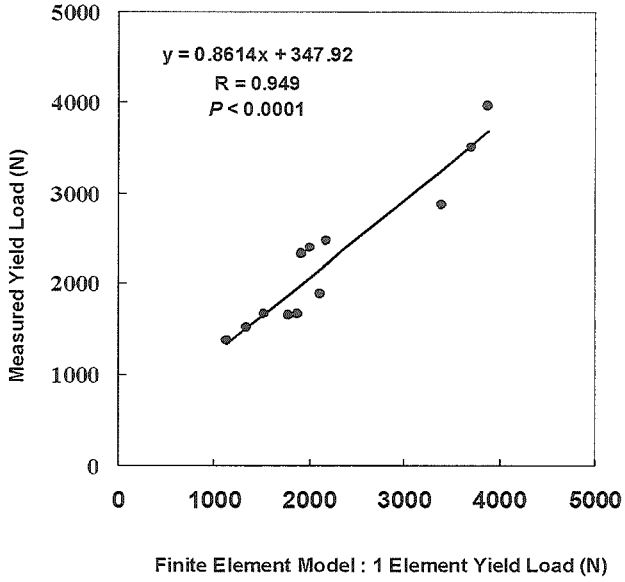
y = 0.8614x + 347.92
R = 0.949
P < 0.0001
Measured Yield Load (N)
Finite Element Model : 1 Element Yield Load (N)
0
1000
2000
3000
4000
5000

Fig. 5

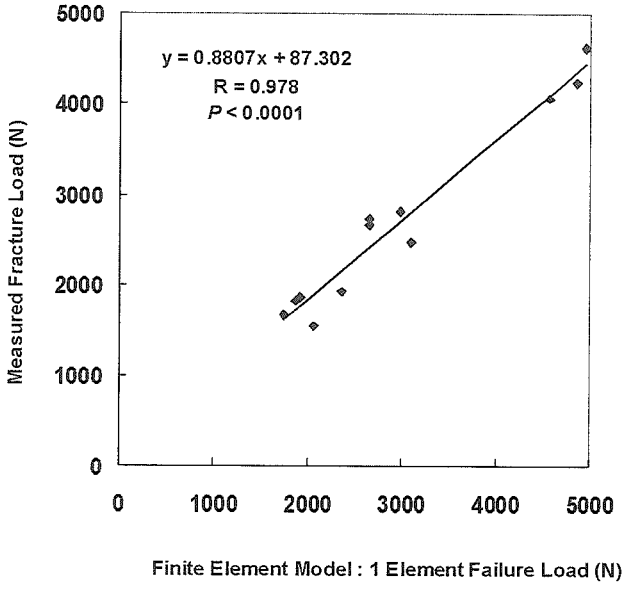
y = 0.8807x + 87.302
R = 0.978
P < 0.0001
Measured Fracture Load (N)
Finite Element Model : 1 Element Failure Load (N)
0
1000
2000
3000
4000
5000